CLM-P735

UKAEA

Preprint

TEARING MODE TRIGGERING OF DISRUPTIONS IN TOKAMAKS

J. W. EASTWOOD
W. ARTER

CULHAM LABORATORY
Abingdon Oxfordshire

1985

CLM-P 735

TEARING MODE TRIGGERING OF DISRUPTIONS IN TOKAMAKS

J W Eastwood and W Arter

Culham Laboratory, Abingdon, Oxon, OX14 3DB, England

(Euratom/UKAEA Fusion Association)

Abstract

Computations have been made with a three-dimensional reduced MHD model to investigate the triggering of disruptions in tokamaks. We have focussed attention on destabilisation through nonlinear interaction between modes of different helicity. We confirm the rapid growth of m/n = 2/1, 3/2 and other modes for strongly unstable initial conditions, but find saturated final states which are not significantly different from the results of single helicity calculations. Such unstable starting points are anyway not inescapable: we show that much more stable profiles are well within experimental error bars. These factors lead us to conclude that dynamical mode interaction is by itself an insufficient trigger.

(Submitted for publication in Physics of Fluids)

February 1985

1. Introduction

It is widely believed that resistive magnetohydrodynamic (MHD) effects, in the form of tearing modes, play a major role in the disruptive termination of tokamak discharges. A tearing mode involves a change in the topology of magnetic field lines which converts parts of the field energy into kinetic and thermal energy. Typically, the magnetic field is little changed outside a narrow "island region", where the driven fluid motion also tends to be concentrated. MHD theories of disruptions are of two basic kinds: one sort relies on the interaction of transport effects with tearing modes[1,2] and the other invokes the interaction of tearing modes of different helicities[3,4]. (Carreras et al[4] will hereinafter be referred to as CHHW.)

The first assumes the current density at the centre of the tokamak plasma to be limited by sawtooth activity or the accumulation of impurities. In these circumstances, a small increase in total current or change in the spatial variation of the resistivity may lead to a situation where the magnetic islands just keep on growing, provided the associated transport effects are allowed to feed back into the resistivity. Ultimately the islands become so large that collectively they cover the effective plasma minor radius, and the associated thermal transport from the centre to the edge then rapidly cools the discharge.

The second argues that a mode with $m/n = 2/1$, where m is the poloidal and n is the toroidal wave number, enters a non-linear regime and destabilises other modes, which then grow explosively fast. CHHW indicates that the interaction of a few modes of low m and n in the

context of reduced MHD[5] is all that is necessary to generate sufficiently wide islands to cool the discharge. Biskamp and Welter[6,7] include O(100) modes in their numerical calculations, so many in fact that they feel able to introduce from turbulence theory the idea of negative effective resistivity to explain the violent behaviour they discover. Drake and Kleva[8] appear to require only the nonlinear self-interaction of the 2/1 mode. The actual resistivity used is independent of time which is why we group these authors' work with that of CHHW, for whom it is inessential that resistance be a function of time to trigger the disruption.

We shall show that when the electrical resistivity η varies only with position, a crucial part is left out of the story of how disruptions are caused. In the reduced MHD equations, an equilibrium field distribution without bulk fluid motion is effectively defined by η : the profiles of safety factor and current density may be trivially derived from knowledge of η as a function of the minor radius r . Since the $\eta(r)$ assumed by the purely MHD papers is very unstable to the growth of the 2/1 mode, it is hard to see how the equilibrium it defines could arise in actual experiments. Ref 8 argues that it arises as a result of a sequence of soft disruptions, which we regard as begging the question. CHHW derive their η by interpreting data from the PLT device. We shall show that another η -profile is equally consistent with experiment, and demonstrate that perturbations to the corresponding equilibrium evolve very differently.

2. The Model and Numerical Techniques

The solely MHD mechanism is studied using the reduced equations of Strauss[5], to which we add a plasma viscosity, so that they become

$$\left(\frac{\partial}{\partial t} + \underset{\sim}{v}\cdot\nabla\right)\psi = \eta J_\zeta - \frac{\partial \phi}{\partial \zeta} - E_\zeta$$

$$\left(\frac{\partial}{\partial t} + \underset{\sim}{v}\cdot\nabla\right)U = - S^2 \left(\underset{\sim}{e}_\zeta \cdot \nabla\psi \times \nabla J_\zeta + \frac{\partial J_\zeta}{\partial \zeta}\right) + p_m \nabla_\perp^2 U \quad .$$

ψ is the dimensionless poloidal magnetic flux function, U is the negative of toroidal vorticity and the other quantities are as defined by Hicks et al[9] except for $p_m = \nu/\eta_0$ where ν is the plasma viscosity (assumed uniform) and η_0 is a typical (dimensional) value of resistivity.

Nonlinear effects are an integral part of the purely MHD mechanism and moreover, the electrical conductivity of present day tokamaks as measured by the Lundquist number S is very high, $S \simeq 10^7 - 10^8$. Thus, the mechanism is studied by numerical calculations which push large computers to their limits, even when the above equations are used and $S = 10^6$.

A code has been produced which owes much to that used by CHHW (see Hicks et al[9]), but with a different time integration scheme. Full details are given by Eastwood and Arter[10] , who derive a sufficient criterion for stability of the numerical algorithm of the form

$$\frac{1}{2}\left(\sqrt{3}\ S\ \left|\underset{\sim}{k}\cdot\underset{\sim}{B}\right| + \left|\underset{\sim}{k}\cdot\underset{\sim}{v}\right|\right)\Delta t \leqslant 1$$

where $\underset{\sim}{k}$ is wavenumber and $\underset{\sim}{v}$ and $\underset{\sim}{B}$ are respectively velocity and magnetic field. Moreover in this companion paper, we show that, as the non-physical change in total energy ΔE (defined below) tends to zero, exact solutions of the modal equations are approached. The modal equations are derived from the governing partial differential system by finite truncation of the Fourier expansion in m/n modes. (Note that structural stability is therefore not guaranteed by $\Delta E \to 0$.) Another natural addition to the code is the facility to calculate and output integral quadratic quantities, such as total magnetic energy, viscous dissipation etc: this we have done.

3. Results Using Initial Profiles of CHHW

3.1 Multi-helicity calculations

The initial profiles of q and current density j adopted by CHHW are those shown in figure 5b. The boundary conditions at r = a ensure that it is a flux surface and the total (toroidal) plasma current is conserved.

It appears that ΔE may become comparable with the total energy when dissipation becomes small, ie S becomes large and p_m tends to zero. Figure 1 illustrates such a case for $p_m = 0$ and $S=10^6$, where S is defined using the value of η at r=0. The island widths shown are the equivalent single helicity island widths as defined by CHHW[4]. The islands grow linearly with time until they overlap, when nonlinear interactions between modes of different helicities become significant.

Figure 1b shows the loop voltage at $r = a$, measured in two different ways. The direct measure V_1 is the value of dimensionless electric field

$$V_1 = E_\zeta \equiv \frac{W_p}{2\pi I}$$

and the indirect measure uses energy conservation and the relationship between the Poynting flux W_p, current I and voltage

$$V_2 = - \frac{\left(\dot{KE} + \dot{ME} + W_J + W_v\right)}{2\pi I} ,$$

where $\dot{KE}$ and $\dot{ME}$ are respectively the rate of change of total kinetic and magnetic energies and W_J is the total Joule dissipation. V_2 differs from the voltage defined by Eq (25) of CHHW by the addition of a dissipation power, W_v arising from the viscous term in the vorticity equation. In the absence of errors in the energy, V_1 and V_2 would be identical, since then

$$\frac{d}{dt} \Delta E = \dot{KE} + \dot{ME} + W_J + W_v + W_p \equiv 0 .$$

In practice, even in the limit $\Delta t \to 0$,

$$\Delta E = \int_0^t dt \left\{\dot{KE} + \dot{ME} + W_J + W_v + W_p\right\}$$

is nonzero due to numerical errors introduced by the discretization in the radial direction. V_2 is no longer identical to V_1:

$$V_1 = V_2 + \frac{\dot{\Delta E}}{2\pi I} \quad .$$

(The truncated spectral (Galerkin) discretization of the toroidal and poloidal co-ordinate dependences does not contribute to ΔE.)

We therefore deduce that shortly after island overlap, the results shown in figure 1 no longer provide an accurate representation of the solution of the resistive Strauss equations[3,5]. Physical and numerical effects conspire to cause the voltage difference. Island overlap generates Alfvén wave transients. Non-linear coupling cascades their energy to wavelengths smaller than the radial mesh spacing and numerical (aliasing) error provides positive feedback to long wavelengths. Sharp gradients develop in the fields and the run then terminates because Δt effectively decreases to zero in order to satisfy the stability criterion. The positive feedback can be suppressed by eliminating aliasing or by increasing physical dissipation to inhibit energy flow to short wavelengths.

Figure 2 shows that introducing viscosity so that $p_m = 1$, together with dropping S from 10^6 to 10^4 enables the computation to be taken beyond the stage of rapid time-dependence (in fact it reduces ΔE to round-off level). We see from figure 2a that the islands saturate at later times, at a total width of about 40% of the plasma minor radius. However, we must remember that the results for large time have limited

physical relevance because of the presence of overlapping islands, and hence enhanced particle (and also thermal) transport. This will at least cause changes in η (if it does not cause the rapid loss of heat that we identify with a disruption) which are not modelled by the reduced MHD equations. We wish here to use figures 1 and 2 only to make the point that transients in the magnetic field distribution are associated with changes in loop volts and that this merely reflects Maxwell's equation curl $\underset{\sim}{E} = -\dot{\underset{\sim}{B}}$.

It may be questioned whether $S = 10^4$ is large enough to simulate tokamak behaviour adequately[6]. Output from runs with $(S,p_m) = (10^6,100)$ and $(10^6,10)$ shares many of the same features as that at $(10^4,1)$. A notable difference is that ΔE rises to be comparable with the energy in the higher order modes: we do not think it remarkable that the larger amplitude of the transient oscillations leads to the loop voltage changing sign. Reducing p_m to unity at $S = 10^6$ leads to $\Delta t \to 0$. Biskamp and Welter[6] also have difficulties at about this point in parameter space. In their case, numerical dissipation appears sufficient to prevent Δt becoming vanishingly small. Our calculations typically use only a small number $N = 11$ of helical modes (Table I), but there are always at least 100 radial mesh-points. Employing 57 modes at $(10^4,1)$ confirms the gross features of our 11-mode result, although admittedly leaving unanswered many questions about high S and low P_m. However, it will become apparent that their solution is in any case irrelevant to the main argument of this paper.

3.2 Single Helicity Calculations

We have used our code to study what happens when the nonlinear interaction between modes of different helicity, which plays such an important role in the purely MHD theory of disruptions, is suppressed. Figure 3 is a superposition of output from two separate computations. In each were allowed only modes of a single helicity, ie modes with wavenumbers of form $p(m_0/n_0)$ where m_0 and n_0 are fixed and p is any integer. (Modes of different helicity are not excited if a calculation is begun with only one helicity.) The figure shows that the calculation with $m_0/n_0 = 2/1$ has the same order of magnitude loop voltage swing and almost the same final 2/1 island width as the multihelical results of figure 2. The final 3/2 island width is reduced in the single helicity case, but this will cause little qualititative change as the 2/1 and 3/2 islands overlap in both instances. (The other modes in the single helicity calculations contain significantly less energy and do not evolve a tearing structure, but reach equilibrium on the time-scale of saturation of the $p = 1$ island.)

We infer from these results that the initial rapid growth of, in particular the 2/1 island, is the consequence of an initial, stagnant equilibrium which is linearly very unstable to the 2/1 and 3/2 modes. Nonlinear coupling does lead to an increased transient growth rate of the 3/2 mode (cf figure 2). However, both with and without nonlinear coupling between 2/1 and 3/2 helicities, the final state at $S = 10^4$ arising from the strongly unstable initial conditions is large overlapping islands. It is then natural to consider why CHHW chose the starting point we have been looking at.

4. Results Using New Initial Profiles

4.1 Experimentally Derived Current Profiles

CHHW's initial conditions are from the interpretation of PLT data obtained just prior to disruption[11]. We have reanalysed this data in quite a simple-minded way, but which, given the error bars on figure 4, a copy of figure 17 of Ref 11, seems as good as any. We make the customary assumptions that the toroidal electric field is uniform and that the plasma is at rest and obeys an Ohm's law with resistivity after Spitzer[12], so that $\eta \propto T_e^{-3/2}$ where T_e is the electron temperature.

The experimental electron temperature (T_e) data was symmetrised about $r = 0$ and used to produce a current density profile, which is, by the above assumptions, proportional to the reciprocal of the resistivity profile. Integrating j gives the q profile. To provide a direct comparison with the strongly unstable profile suggested by CHHW, we perform a three parameter fit using the parametric formula favoured by CHHW: $q(r) = q_0\left(1 + (r/r_0)^{2\lambda}\right)^{1/\lambda}$. The resulting q profile and current density profile $j(r)$ are plotted in figure 5a ($q_0 = 0.7$, $r_0 = 0.48$, $\lambda = 1.5$). The arrows indicating the positions of the $q = 1$, 2 and 3 surfaces on figure 5 correspond to the locations of those surfaces as derived from the data shown in figure 4.

The value of $q_0 = 0.7$ on axis is inconsistent with the view that $m = 1$ instabilities will keep $q \gtrsim 1$ on axis. However, this value arose from the combination of the assumptions of axisymmetry, Spitzer reistivity

and uniform electric field. Relaxing the axisymmetry and uniform field assumptions (as the nonlinear calculation does) rapidly flattens q to $q \simeq 1$ inside the $q = 1$ surface (cf Sec 3.3 below and Figure 5a).

Figure 5b shows the quite different q and current density profiles used by CHHW[4] where $q_0 = 1.34$, $r_0 = 0.567$ and $\lambda = 3.24$. These values were also used for the calculations presented in figures 1-3. This interpretation of j has a flatter top more like experimental data, but the corresponding q is everywhere greater than 1.34, whereas the equilibrium of figure 5a contains a $q = 1$ surface in agreement with the soft X-ray data[11]. Note that the q profiles of figures 5a and 5b agree closely for radii $r > 0.6a$. The effect of taking the larger q_0 and λ is to make the j profile flat topped, with steeper current gradients at the $q = 2$ and 3 surfaces compared to figure 5a.

4.2 The New Profile as Initial Conditions

It is not surprising that the equilibrium of figure 5a leads to very different results from those of figure 5b. Linear analysis and single helicity calculations[13] suggest that the current profile in figure 5a is unstable to $m/n = 1/1$ modes, whereas the steeper gradients of j shown in figure 5b are unstable to tearing modes at the $q = 2$ and 3 surfaces[14]. The nonlinear computations bear this out.

The only difference between the calculations shown in figures 2 and 6 is the initial q profile: in both cases $(S, p_m) = (10^4, 1)$ and even the

perturbations are identical. In figure 6, the 2/1 and 3/2 islands fade away, and the 1/1 mode grows to flatten q inside the $q = 1$ surface. The final q profile is shown superimposed on the initial one in figure 5a. A voltage spike arising from the unstable initial conditions is seen as the 1/1 island grows. This behaviour of the voltage parallels that seen as the 2/1 and 3/2 islands grow in the figure 2 case.

5. Conclusions

We have undertaken computational studies of the nonlinear interaction of tearing modes of different helicities. Our numerical model is such that we are always able to ensure linear numerical stability. In the limit where the Lundquist number becomes large and the magnetic Prandtl number becomes small, the code fails to conserve energy and in extreme cases the stability criterion causes the timestep to become vanishingly small. This we attribute to nonlinear interactions cascading Alfven wave energy to subgrid scalelengths and the return of this energy by numerical effects back to long wavelengths. We have shown that this totally spurious feedback is vitiated by letting our plasma model be slightly viscous, since this inhibits the flow of Alfvén wave energy to subgrid scalelengths.

We have computed the evolution of tearing modes for the initial profiles used by CHHW[4]. Current conserving boundary conditions were imposed on the conducting wall boundary and transport processes were not included. Our results confirm that tearing modes grow in current profiles which are unstable to tearing modes. If we restrict parameters to those for which we can demonstrate convergence (ie ΔE at roundoff level), then

the islands saturate at large but finite widths. Physically, the neglect of transport becomes dubious as the magnetic islands reach this kind of size. Nevertheless, we think it worthwhile to point out that within the context of the model equations, apart from a transient oscillatory transfer of energy between different helicities, the multihelical results do not differ qualitatively from superimposed single helicity results. In both cases we observe that unstable tearing modes grow to saturation and that similar loop voltage transients occur.

We draw attention to the basic fact that magnetic field transients normally lead to changes in the voltage across a system. The changes in loop voltage seen in the calculations of Carreras et al[4] and of Biskamp and Welter[6] reflect the fact that the magnetic field distribution is changing rapidly. The field is changing rapidly because the initial current profile used in their calculations is very unstable to tearing mode growth. It is a side issue here whether their or our numerically calculated voltages are sufficiently accurate.

The unstable initial profile was obtained by interpreting experimental data. We have shown that other profiles are also consistent with that data: including one which is stable to the growth of 2/1 and 3/2 modes. It seems to us essential to let j or correspondingly η evolve consistently with even some fairly simple transport model. Demonstrating that tearing modes grow rapidly from initial axisymmetric current profiles which are strongly tearing mode unstable does not address the fundamental question, viz what physical mechanism gives rise to these profiles. We suggest that the triggering of disruptions needs to be explained in terms of the interaction of transport and MHD instability.

References

1 Turner M F and Wesson J A 1982 Transport, instability and disruptions in tokamaks. Nucl Fus 22, 1069-1078

2 Wesson J A, Sykes A and Turner M F 1982 Tokamak disruptions. CLM-R233

3 Waddell B V, Carreras B A, Hicks H R, Holmes J A and Lee D K 1978 Mechanism for major disruptions in tokamaks. Phys Rev Lett 41, 1386-1389

Waddell B V, Carreras B, Hicks H R and Holmes J A 1979 Nonlinear interaction of tearing modes in highly resistive tokamaks. Phys Fluids 22, 896-910

4 Carreras B A, Hicks H R, Holmes J A and Waddell B V 1980 Nonlinear coupling of tearing modes with self-consistent resistivity evolution in tokamaks. Phys Fluids 23, 1811-1825

5 Strauss H R 1976 Nonlinear three-dimensional magnetohydrodynamics of noncircular tokamaks. Phys Fluids 19, 134-140

6 Biskamp D and Welter H 1983a Studies of MHD turbulence in low-β current-driven plasmas, pp373-381 in Plasma Physics and Controlled Nuclear Fusion Research 1982, Vol III, IAEA, Vienna

7 Biskamp D and Welter H 1983b Negative anomalous resistivity - a mechanism of the major disruption in tokamaks. Phys Lett 96A, 25-28

8 Drake J F and Kleva R G 1984 Are major disruptions in tokamaks caused by vacuum bubbles? Phys Rev Lett 53, 1465-1468

9 Hicks H R, Carreras B A, Holmes J A, Lee D K and Waddell B V 1981 3-D nonlinear calculations of resistive tearing modes. J Comp Phys 44, 46-69 (Erratum 1984 J Comp Phys 53, 205)

10 Eastwood J W and Arter W 1985. In preparation

11 Sauthoff N R, van Goeler S and Stodiak W 1978 A study of disruptive instabilities in the PLT tokamak using X-ray techniques. Nucl Fus 18, 1445-1458

12 Spitzer L 1956 The Physics of Fully Ionised Gases, Interscience, New York

13 Waddell B V, Rosenbluth M N, Monticello D A and White R B 1976 Nonlinear growth of the m = 1 tearing mode. Nucl Fus 16, 528-532

14 Furth H P, Rutherford P H and Selberg H 1973 Tearing modes in the cylindrical tokamak. Phys Fluids 16, 1054-1063

Table I

Modes m/n used when N = 11					
			n		
	0	1	2	3	4
m					
8					x
7					x
6				x	x
5				x	
4			x		
3			x		
2		x			
1	x	x			
0	x				

Modes m/n used when N = 57										
					n					
	0	1	2	3	4	5	6	7	8	9
m										
8			x	x	x	x	x	x	x	x
7			x	x	x	x	x	x	x	
6			x	x	x	x	x	x		
5	x	x	x	x	x	x				
4	x	x	x	x	x	x				
3	x	x	x	x	x	x				
2	x	x	x	x	x	x				
1	x	x	x	x	x	x				
0	x	x	x	x	x	x				

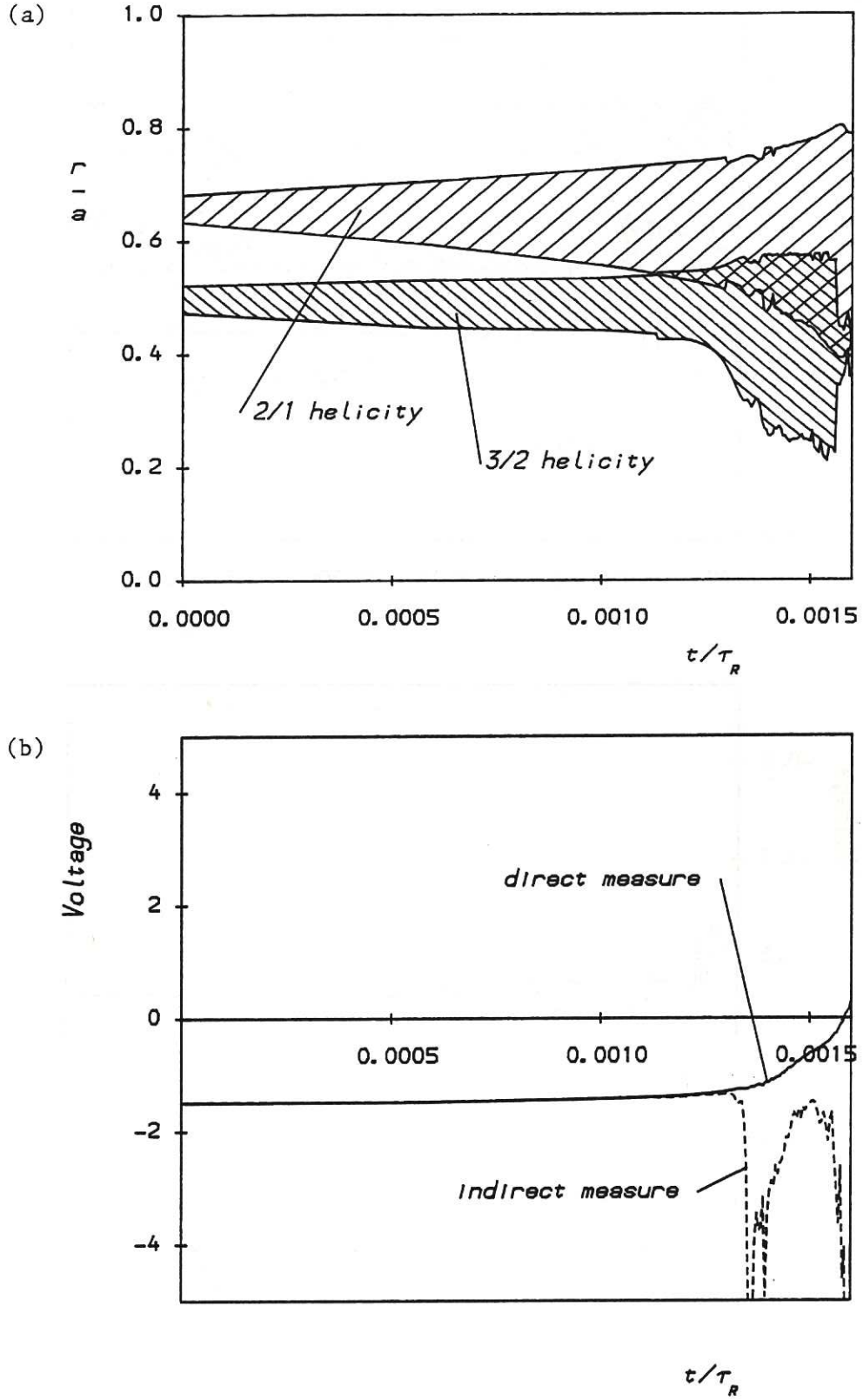

Fig. 1(a) Time-dependence of island widths w (as defined by CHHW) for $S = 10^6$ and $p_m = 0$. For clarity, not all $w \neq 0$ are plotted. Time is measured in units of $\tau_R = a^2/\eta_0$, radial co-ordinate r in units of a, where a is the plasma minor radius. Note the strange behaviour of the 3/2 island width just before the calculation terminates.

(b) Dimensionless loop voltage as a function of time. The indirect measure (V_2) assumes energy conservation.

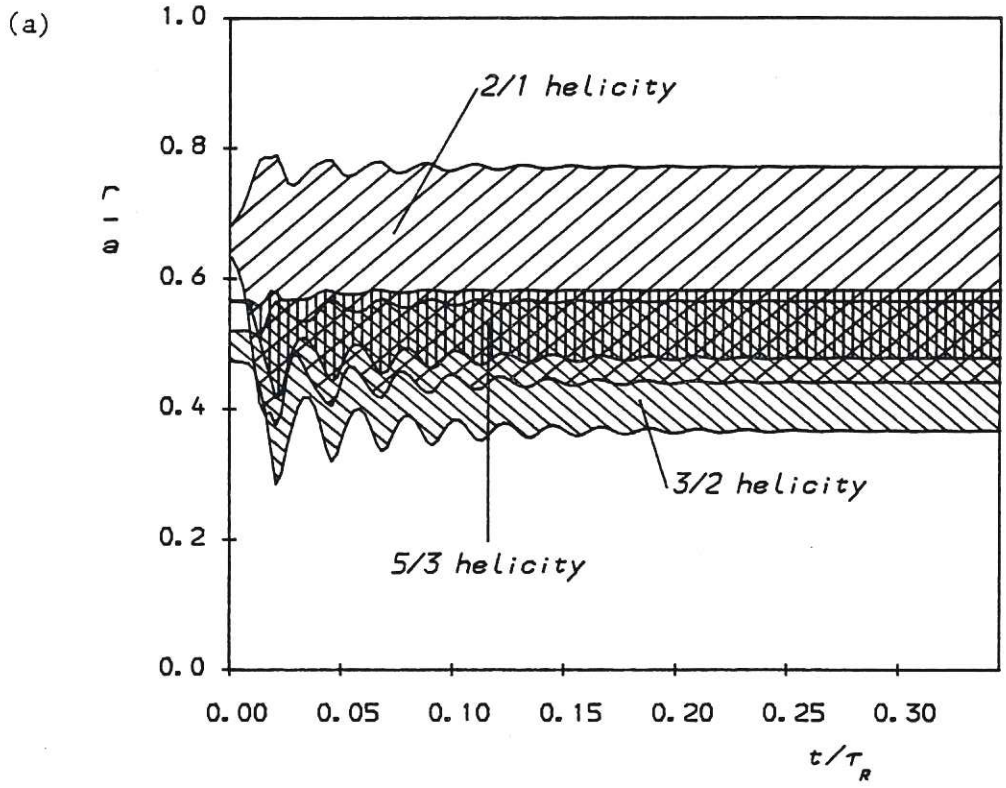

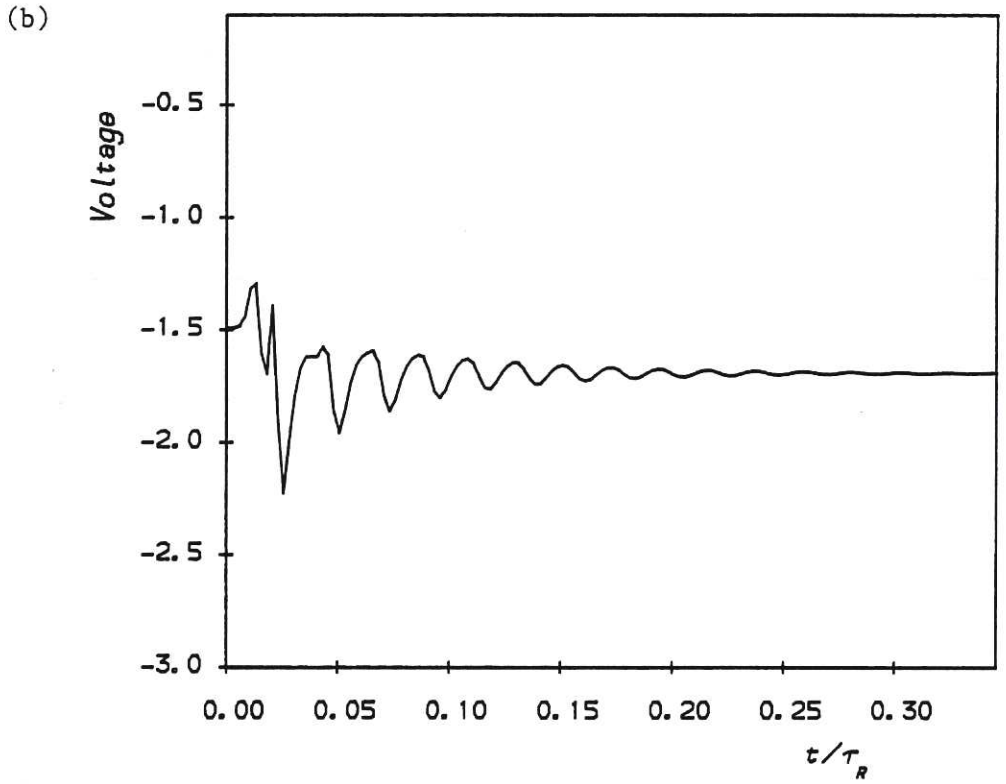

Fig.2 As Figure 1, except now $S = 10^4$, $p_m = 1$. In (b) the indirect and direct measures of loop voltage are indistinguishable.

(a)

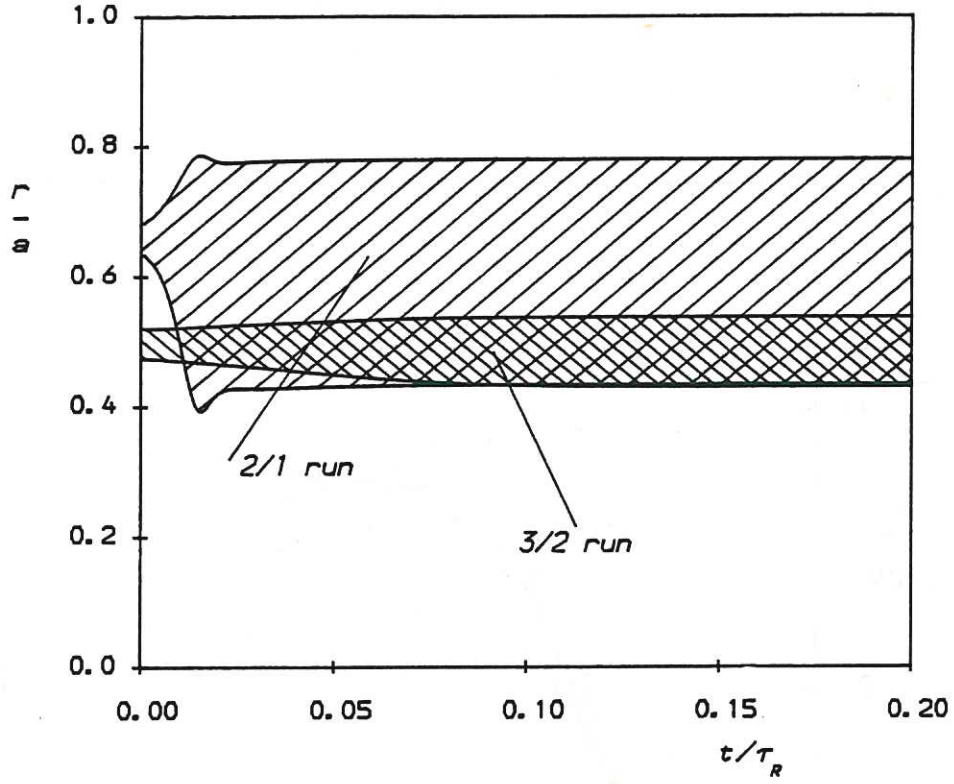

(b)

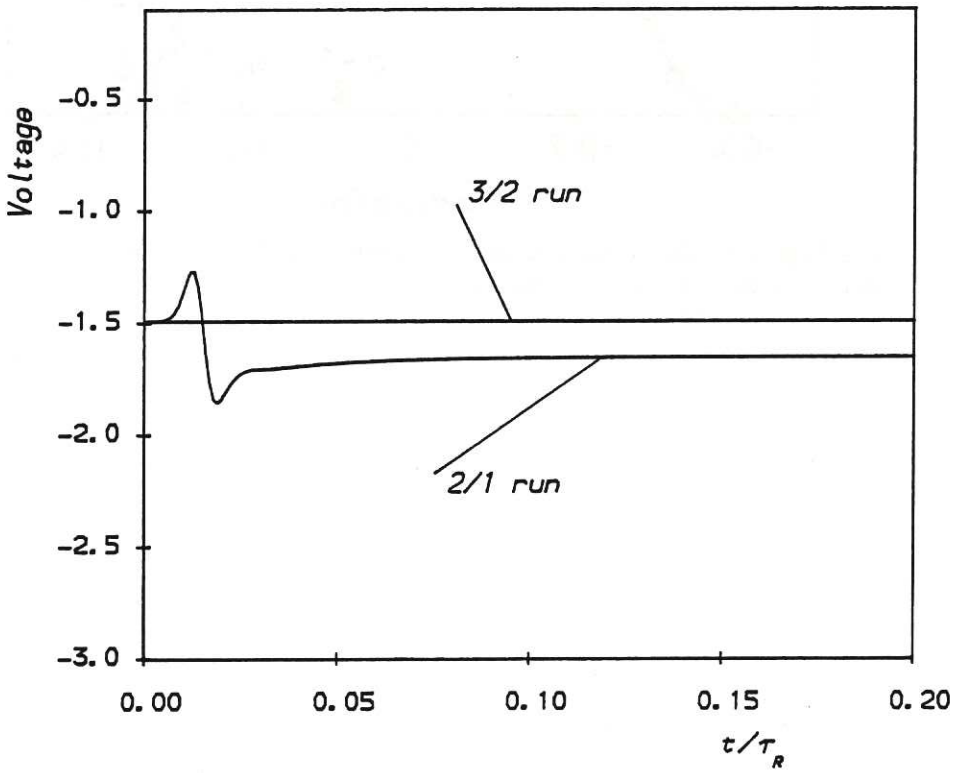

Fig.3 As Figure 1, except now $S = 10^4$, $p_m = 1$ and output from two single-helicity computations is superimposed. All non-zero w are shown.

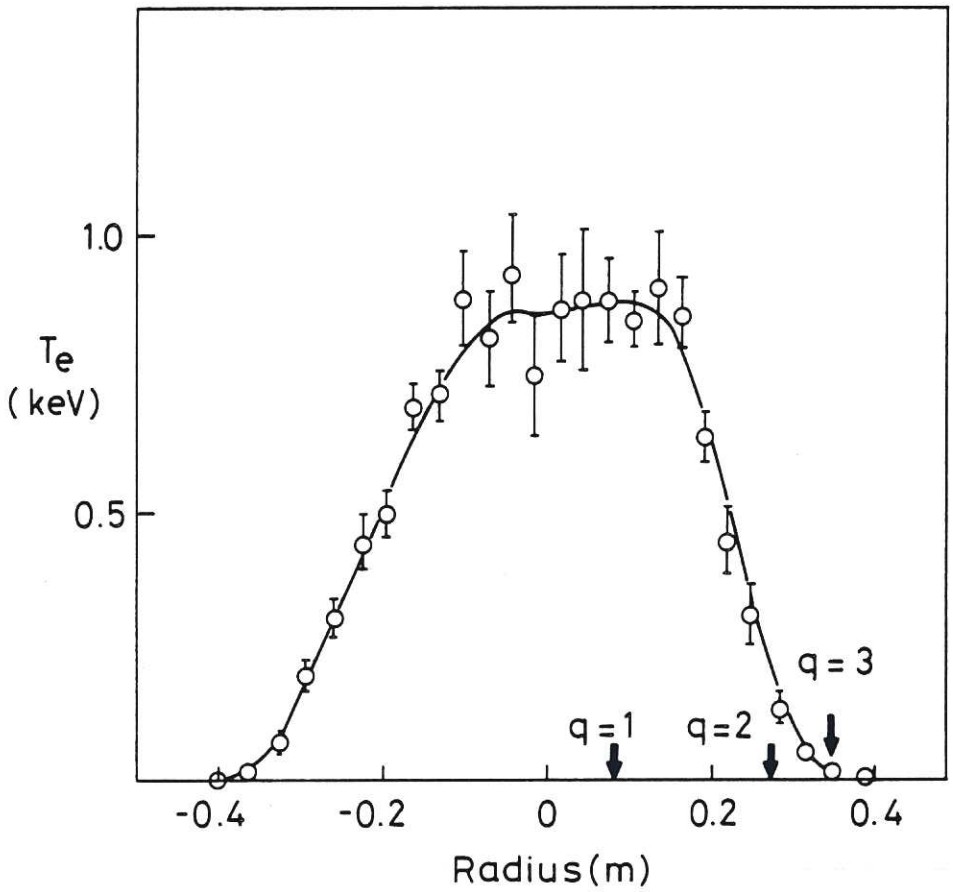

Fig.4 Experimentally measured temperature profile from PLT data, based on Figure 17 of Ref. 11. The arrows mark the position of the q surfaces derived from soft X-ray measurements.

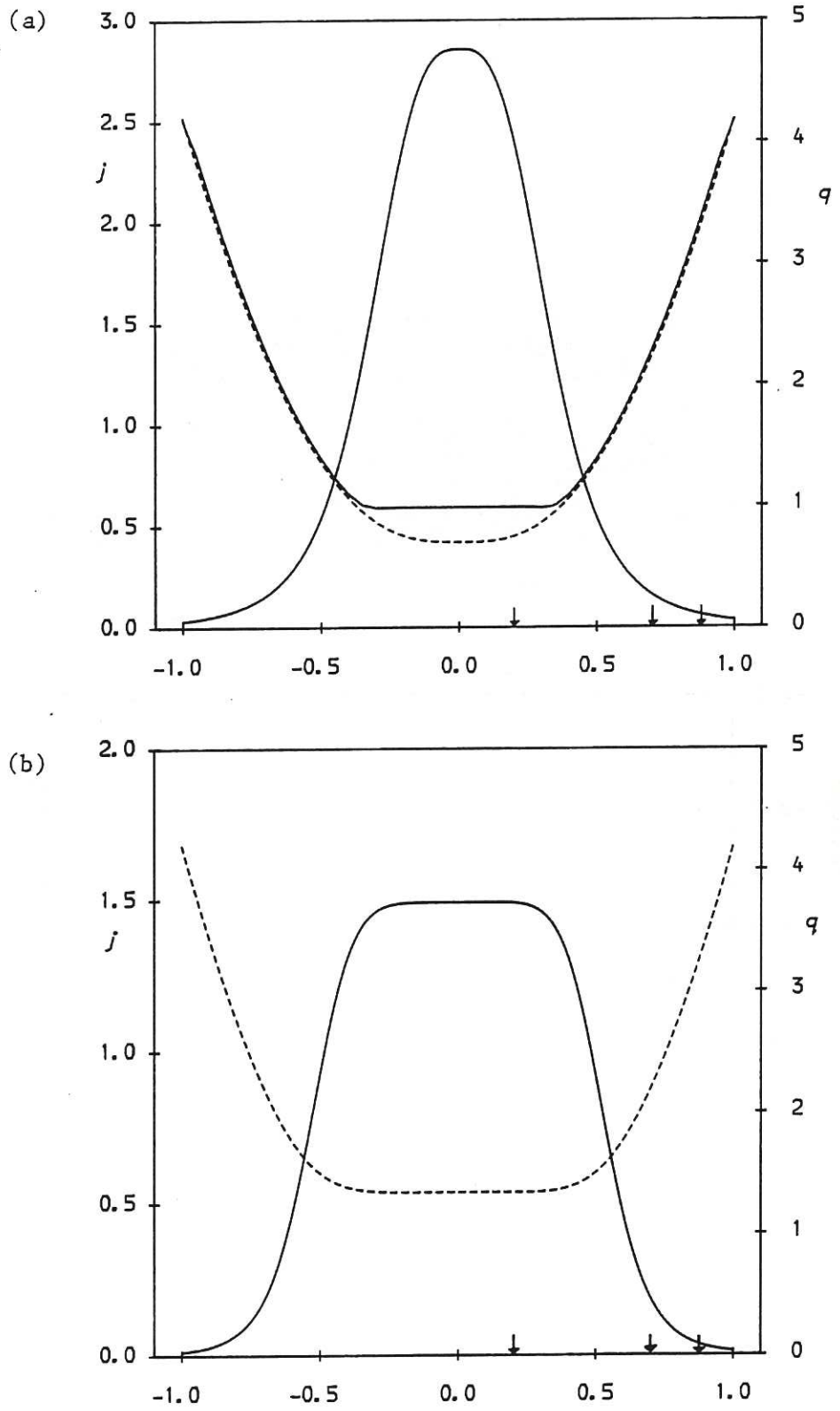

Fig.5 Safety factor profiles $q(r, q_0, r_0, \lambda)$ drawn dashed, and the corresponding dimensionless current densities $j(r)$. The normalisation of j is chosen such that the same total current flows in each case. (a) $q_0 = 0.7$, $r_0 = 0.48$ and $\lambda = 1.5$; (b) $q_0 = 1.34$, $r_0 = 0.567$ and $\lambda = 3.24$. (a) also shows the q profile after tearing modes have saturated. The arrows correspond in relative position to those drawn in Figure 4.

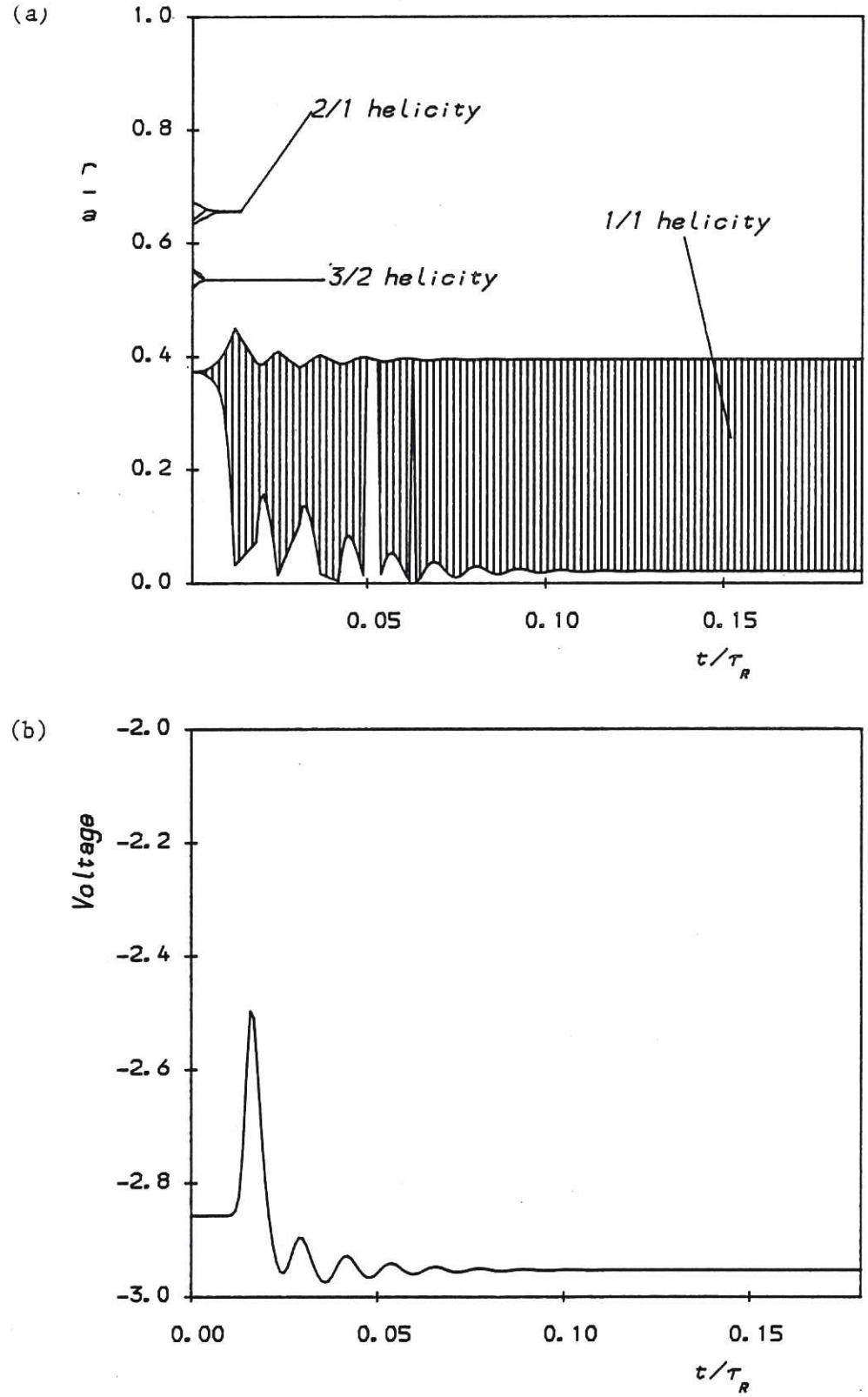

Fig. 6 As Figure 1, except now $S = 10^4$, $p_m = 1$, different initial conditions and all non-zero w are shown. The peculiar behaviour of the 1/1 island width is an artefact of the plotting routine.